Brazilian Journal of Physics
ISSN: 0103-9733
luizno.bjp@gmail.com
Sociedade Brasileira de Física
Brasil

Engelbrecht, N. E.; Burger, R. A.
Cosmic-Ray Modulation: an Ab Initio Approach
Brazilian Journal of Physics, vol. 44, núm. 5, 2014, pp. 512-519
Sociedade Brasileira de Física
Sâo Paulo, Brasil

Braz J Phys (2014) 44:512–519
DOI 10.1007/s13538-014-0241-7

PARTICLES AND FIELDS

Cosmic-Ray Modulation: an Ab Initio Approach

N. E. Engelbrecht · R. A. Burger

Received: 5 June 2014 / Published online: 4 September 2014

Abstract A better understanding of cosmic-ray modulation in the heliosphere can only be gained through a proper understanding of the effects of turbulence on the diffusion and drift of cosmic rays. We present an ab initio model for cosmic-ray modulation, incorporating for the first time the results yielded by a two-component turbulence transport model. This model is solved for periods of minimum solar activity, utilizing boundary values chosen so that model results are in fair to good agreement with spacecraft observations of turbulence quantities, not only in the solar ecliptic plane but also along the out-of-ecliptic trajectory of the Ulysses spacecraft. These results are employed as inputs for modelled slab and 2D turbulence energy spectra. The latter spectrum is chosen based on physical considerations, with a drop-off at the very lowest wavenumbers commencing at the 2D outerscale. There currently exist no models or observations for this quantity, and it is the only free parameter in this study. The modelled turbulence spectra are used as inputs for parallel mean free path expressions based on those derived from quasi-linear theory and perpendicular mean free paths from extended nonlinear guiding center theory. Furthermore, the effects of turbulence on cosmic-ray drifts are modelled in a self-consistent way, employing a recently developed model for drift along the wavy current sheet. The resulting diffusion coefficients and drift expressions are applied to the study of galactic cosmic-ray protons and antiprotons using a three-dimensional, steady-state cosmic-ray modulation code, and sample solutions in fair agreement with multiple spacecraft observations are presented.

Keywords Turbulence · Diffusion · Drift · Cosmic-ray modulation

N. E. Engelbrecht (✉) · R. A. Burger
Center for Space Research, North-West University, Potchefstroom, South Africa
e-mail: 12580996@nwu.ac.za

1 Introduction

Numerical cosmic-ray (CR) modulation studies are concerned with calculating the CR differential intensity $j=P^2 f_0$, where $f_0(\mathbf{r}, p, t)$ is the omnidirectional CR distribution function in terms of particle momentum p, using the Parker transport equation (TPE) given by [30]

$$\frac{\partial f_0}{\partial t} = \nabla\cdot(\mathbf{K}\cdot\nabla f_0) - \mathbf{V}\cdot\nabla f_0 + \frac{1}{3}(\nabla\cdot\mathbf{V})\frac{\partial f_0}{\partial \ln p} + Q, \tag{1}$$

where V denotes the solar wind speed, P particle rigidity, Q any sources of CRs in the heliosphere, and $\mathbf{K}$ the diffusion tensor. The above TPE describes various processes which act so as to modulate an initial interstellar cosmic-ray distribution function. These processes, in the order in which the terms governing the processes appear on the right hand side of Eq. 1, are diffusion and drift due to gradients and curvature of the heliospheric magnetic field (HMF), the effects of outward convection of CRs due to the action of the solar wind and adiabatic cooling.

The force field approximation [15] is still used to solve the Parker TPE: assuming a steady state, no sources, zero explicit adiabatic energy loss rate and spherical symmetry, the Parker TPE becomes [27]

$$CV\ f_0 - \kappa d\ f_0/dr = 0, \tag{2}$$

where κ is some diffusion coefficient, and C the Compton-Getting factor. The solution to the above is relatively straightforward. Assuming that $\kappa(r, P)=\beta\,\kappa_1(r)\kappa_2(P)$,

$$j(r,E) = \left|\frac{E^2 - E_0^2}{(E+\Phi)^2 - E_0^2}\right| j_{LIS}(E+\Phi) \tag{3}$$

with $\Phi=Ze\phi$, where $\phi(r) = \int_r^{r_B} \frac{V(r')}{3\kappa_1(r')} dr'$. Note that E_0 is the rest-mass energy of the cosmic-ray species in question, and j_{LIS} its local interstellar intensity. However, such simplicity comes at a price. Much of the physics underlying CR modulation is

ignored in the force-field approach: information about the diffusion tensor is lost, and drift effects can't be taken into account.

In a more general approach, the diffusion tensor can be expressed in HMF-aligned coordinates as

$$\mathbf{K}' = \begin{bmatrix} \kappa_{\parallel} & 0 & 0 \\ 0 & \kappa_{\perp,2} & \kappa_A \\ 0 & -\kappa_A & \kappa_{\perp,3} \end{bmatrix}. \quad (4)$$

Here, $\kappa_{\perp,2}$ and $\kappa_{\perp,3}$ describe diffusion in directions perpendicular to the HMF, $\kappa_{\parallel}$ describes diffusion parallel to the field, and κ_A denotes the drift coefficient. These coefficients can be expressed in terms of mean free paths (MFPs), such that, e.g. $\kappa_{\parallel}=(v/3)\lambda_{\parallel}$ with v the particle speed. In the ab initio approach to CR modulation studies, these MFPs must be derived from some scattering theory/theories (such as quasilinear theory [17]), which in turn require turbulence power spectra as key inputs [36]. Such power spectra must be modelled throughout the heliosphere, which can be done by specifying a form for the spectra in question, and using a turbulence transport model (TTM) for the various basic turbulence quantities, these spectra are functions of. Drift effects are also reduced in the presence of turbulence [26], which can be taken into account using outputs yielded by a TTM. In what follows, a brief outline of such an approach to the study of galactic CR modulation is given, with emphasis on the effect that the 2D outerscale has on the diffusion tensor and the computed galactic CR intensities. For a much more complete discussion of this approach and the results presented here, the reader is invited to consult [12, 11].

2 Turbulence Quantities

As outlined above, scattering theories used to derive expressions for CR diffusion coefficients require as inputs expressions for the power spectra of the turbulent fluctuations in the HMF. This study proceeds under the [4] assumption of composite turbulence and assumes that the total turbulence modal spectrum can be expressed as $G(\mathbf{k})=G^{slab}(k_{\parallel})\delta(k_{\perp})+G^{2D}(k_{\perp})\delta(k_{\parallel})$, where $G(\mathbf{k})$ and $G^{2D}(k_{\perp})$ denote the slab and 2D modal spectra, respectively. The slab spectrum is chosen following [40] so that it has a flat energy range and a Kolmogorov inertial range, where

$$G^{slab}(k_{\parallel}) = \begin{cases} g_o k_m^{-s}, & |k_{\parallel}| \le k_m; \\ g_o |k_{\parallel}|^{-s}, & k_m \le |k_{\parallel}| \le k_d; \\ g_1 |k_{\parallel}|^{-p}, & |k_{\parallel}| \le k_d, \end{cases} \quad (5)$$

with k_m and k_d the parallel wavenumbers at which the inertial and dissipation ranges commence. Note that $g_1=g_0 k_d^{p-s}$ and

$$g_o = \left[s + \frac{s-p}{p-1}\left(\frac{k_m}{k_d}\right)^{s-1} \right]^{-1} \frac{\delta B_{sl}^2 k_m^{s-1}(s-1)}{8\pi}. \quad (6)$$

The form of the 2D modal spectrum is chosen following the physical motivations presented by [24]. This spectrum also has an inertial range (that commences at λ_{2D}) and a flat energy-containing range as well as an 'outer range' displaying a steep decrease at the smallest wavenumbers:

$$G^{2D}(k_{\perp}) = g_2 \begin{cases} (\lambda_{out} k_{\perp})^q, & |k_{\perp}| < \lambda_{out}^{-1}; \\ 1, & \lambda_{out}^{-1} \le |k_{\perp}| < \lambda_{2D}^{-1}; \\ (\lambda_{2D} k_{\perp})^{-\nu}, & |k_{\perp}| \ge \lambda_{2D}^{-1}. \end{cases} \quad (7)$$

where $g_2=(C_0\lambda_{2D}\delta B_{2D}^2)/(2\pi k_{\perp})$ and

$$C_0 = \left[\left(1 - \frac{q}{1+q}\left(\frac{\lambda_{2D}}{\lambda_{out}}\right) + \frac{1}{\nu - 1} \right) \right]^{-1}. \quad (8)$$

Note that δB_{2D}^2 and δB_{sl}^2 denote the 2D and slab variances, $\nu=s=5/3$ the spectral indices for both spectra in the inertial range and $q=3$ the spectral index in the 'inner range' of the 2D spectrum. The lengthscale λ_{out} denotes the 2D outerscale where the energy range commences, such that $\lambda_{out}>\lambda_{2D}$. No observations currently exist for this lengthscale, and a simple dependence on the 2D correlation scale $\lambda_{c,2D}$ is employed here. It was found by [12, 11] that a choice of $\lambda_{out}=12.5\lambda_{c,2D}$ results in computed CR intensities in reasonable agreement with spacecraft observations.

The above spectra are functions of various turbulence quantities, which need to be modelled throughout the heliosphere. To this end, the two-component TTM of [28] is employed. This model is solved by [12, 11] for solar minimum conditions, assuming a Parker HMF and choosing with boundary values so as to obtain agreement between computed turbulence quantities and various spacecraft measurements of these quantities throughout the heliosphere.

Figures 1 and 2, taken from [11], show the various turbulence quantities computed with this model in the solar ecliptic plane and along the trajectory of the Ulysses spacecraft. Both these figures show that reasonable agreement can be found with observations using the [28] model, also along the trajectory of Ulysses. Note that, although the correlation scales in the outer heliosphere shown in Fig. 1 are consistently smaller than the Voyager values reported by [23, 38] report, single spacecraft observations of correlation scales tend to overestimate these quantities by a factor of 2–4.

3 Diffusion and Drift Coefficients

The choice of scattering theory to be used to derive MFP expressions from is a vital one in any study of cosmic-ray modulation. This choice is difficult, in that numerical simulations of diffusion coefficients, such as those performed by, e.g. [25, 32], appear to show that there is not, as of yet, a scattering theory that can accurately reproduce the simulated MFPs for

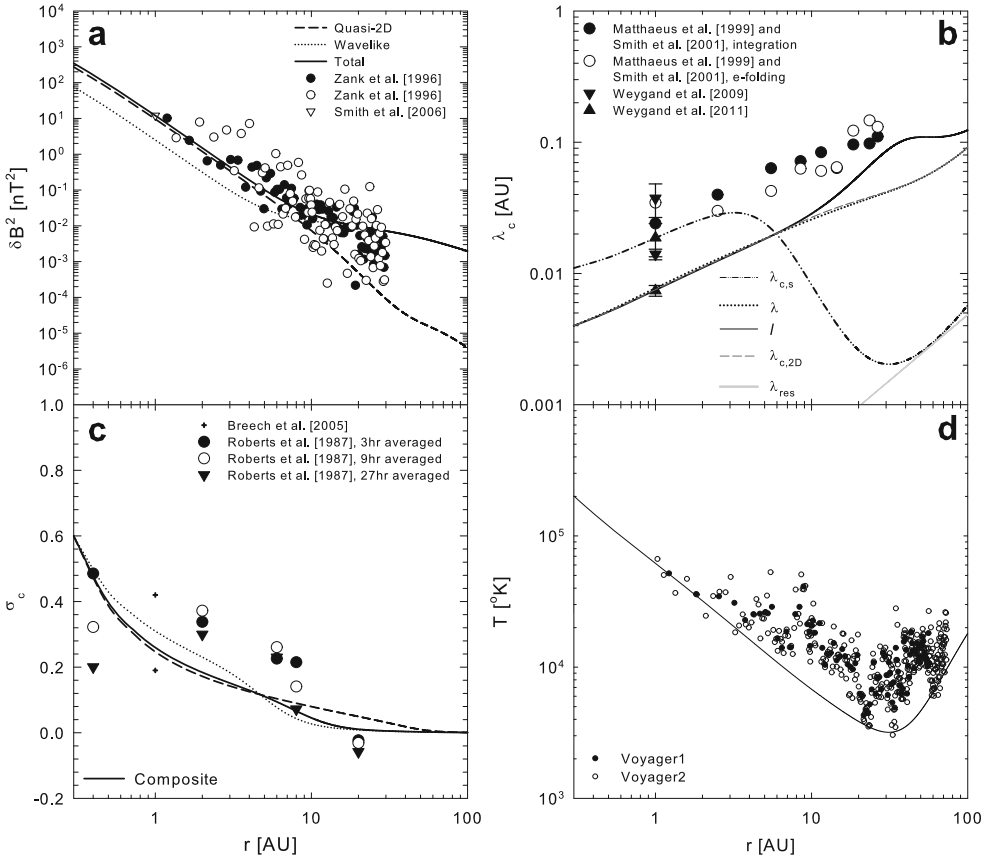

Fig. 1 Various turbulence quantities computed by [12, 11] using the [28] TTM, in the solar ecliptic plane. Figure taken from [11] Turbulence observations shown are reported by [43, 39, 38, 21, 41, 42, 5, 33, 34],

all the turbulence conditions considered in the abovementioned studies. The quasilinear theory (QLT) of [17] is used here model parallel diffusion, employing expressions for the parallel MFP based on the results of [40]. This is motivated by the fact that simulations show that QLT yields reasonable values for the parallel MFP when compared with simulations of $\lambda_\parallel$ for low levels of turbulence [25]. It should be noted that the TTM used here yields low levels of slab turbulence in most of the model heliosphere [11]. The proton parallel MFP expression is constructed by [9] from piecewise continuous expressions derived by [40], such that

$$\lambda_\parallel = \frac{3s}{\sqrt{\pi}(s-1)}\,\frac{R^2}{k_m}\left(\frac{B_o}{\delta B_{sl}}\right)^2 \cdot \left[\frac{1}{4\sqrt{\pi}} + \frac{2R^{-s}}{\sqrt{\pi}(2-s)(4-s)}\right], \quad (9)$$

with $R=R_L k_m$, where R_L is the (maximal) proton gyroradius. Note that the effects of the dissipation range in Eq. 5 are neglected. The extended nonlinear guiding center (ENLGC) theory of [35] is used to derive an expression for the perpendicular MFP from Eq. 7. This theory is based on the NLGC theory of [22] and agrees with simulations for a broad range of turbulence conditions [25, 32, 35]. The perpendicular MFP used here is that derived by [12, 11] and is given by

$$\lambda_\perp = \frac{2a^2}{B_o^2}\,\frac{C_0 \lambda_{2D} \delta B_{2D}^2}{\lambda_\perp}\left[h_{\perp,1} + h_{\perp,2} + _{\perp,3}\right], \quad (10)$$

where

$$h_{\perp,1} = \frac{\lambda_\parallel \lambda_\perp}{(1+q)\lambda_{out}} 2F_1\left(1, \frac{1+q}{2}, \frac{3+q}{2}; -x^{-2}\right),$$

$$h_{\perp,2} = \sqrt{3\lambda_\parallel \lambda_\perp}[\arctan(x) - \arctan(y)],$$

$$h_{\perp,3} = \frac{3\lambda_{2D}}{(1+v)} 2F_1\left(1, \frac{1+v}{2}, \frac{3+v}{2}; -y^2\right),$$

with

$$x = \frac{\sqrt{3}\lambda_{out}}{\sqrt{\lambda_\parallel \lambda_\perp}} \text{ and } y = \frac{\sqrt{3}\lambda_{2D}}{\sqrt{\lambda_\parallel \lambda_\perp}}, \quad (11)$$

The parameter a^2 is a constant set to 1/3 in this study, after [22]. The above expressions are evaluated numerically using the results yielded by the TTM to model turbulence quantities. The turbulence-reduced drift coefficient used in this study is that of [8], based on the work of [3] who find that

$$\kappa_A = \frac{v}{3} R_L \frac{\Omega^2 \tau^2}{1 + \Omega^2 \tau^2}, \quad (12)$$

with τ a decorrelation rate, and Ω the particle gyrofrequency [8] propose a parametrized form for the product $\Omega\tau$,

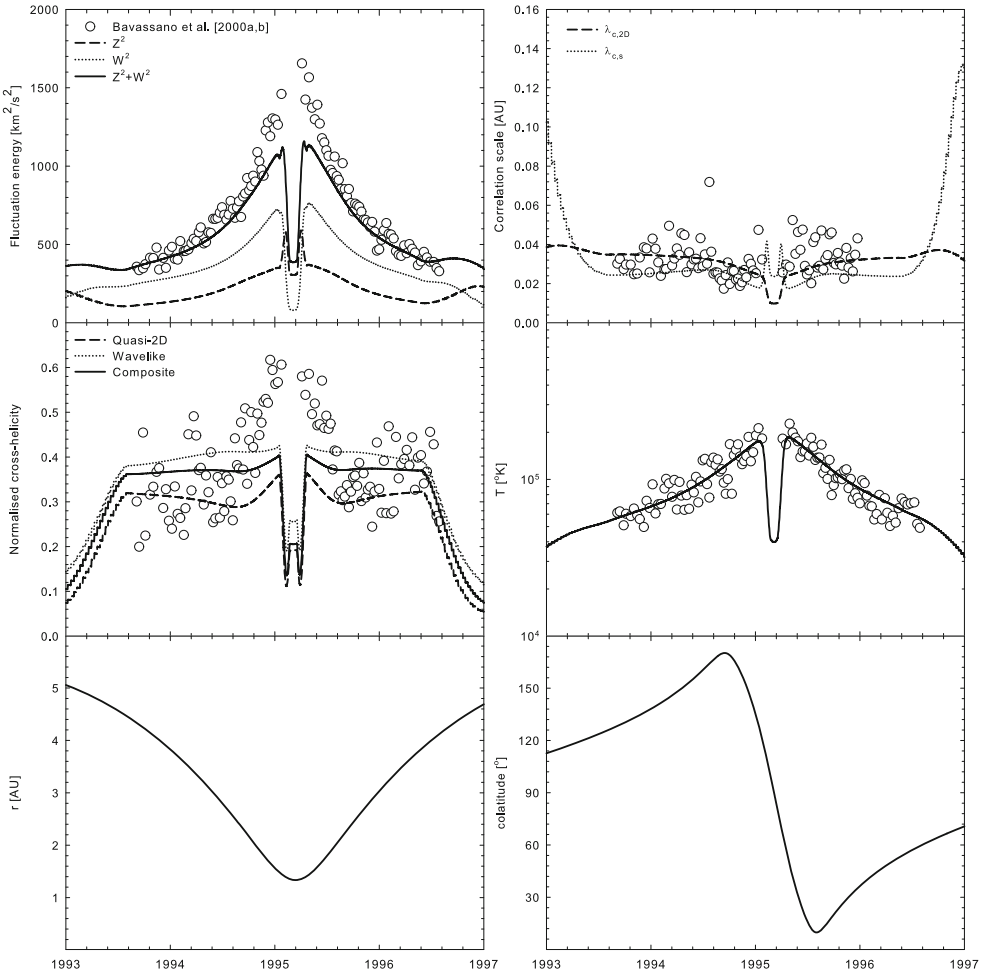

Fig. 2 Various turbulence quantities computed by [12, 11] using the [28] TTM, along the trajectory of the *Ulysses* spacecraft (shown in the *bottom panels*). Figure taken from [11] Turbulence observations shown are reported by [1, 2]

chosen so as to agree with the simulations of [26], and given by

$$\Omega\tau = \frac{11}{3}\frac{\sqrt{R_L/\lambda_{c,s}}}{\left(D_\perp/\lambda_{c,s}\right)^g}, \tag{13}$$

where $g = 0.3\ \log(R_L/\lambda_{c,\ s}) + 1.0$ and $D_\perp = (1/2)\left(D_{sl} + \sqrt{D_{sl}^2 + 4D_{2D}^2}\right)$ the field line random walk diffusion coefficient [20], with $D_{sl} = \left(\delta\ B_{sl}^2/2B_o^2\right)\lambda_{c,s}$ and $D_{2D} = \left(\lambda_u\sqrt{\delta\ B_{2D}^2/2}\right)/B_o$. The quantity $\lambda_{c,\ s}$ is the slab correlation scale, and λ_u the 2D ultrascale [24]. The ultrascale is calculated from the 2D modal spectrum (Eq. 7), following the approach outlined by [24]. Note that all turbulence quantities appearing in the above expressions are modelled using the [28] TTM. Since no direct observations exist for the 2D outerscale λ_{out}, the perpendicular MFP and drift scale will be characterized below on the basis of very simple spatial dependences for this quantity, such that

$$\lambda_{out} = const\lambda_{c,2D} \tag{14}$$

where $\lambda_{c,2D}$ is the 2D correlation scale and *const* is taken to assume values of 10, 100 and 1000. This choice is made to accentuate the effect the magnitude of this quantity may have on the expressions presented above.

The MFPs described by Eqs. 9 and 11, as well as the lengthscale λ_A associated with the drift coefficient, are shown in Fig. 3 as functions of rigidity (top panels), colatitude (middle panels) and heliocentric radial distance (bottom panels), for various simple choices as to the 2D outerscale. The proton parallel MFPs at Earth fall reasonably within the Palmer consensus range [29] but tend to be a bit large, a consequence of the choice of solar minimum turbulence quantities made here. At 1 AU, the parallel MFP displays a $P^{1/3}$ rigidity dependence. At 100 AU, these parallel MFPs display a P^2 rigidity dependence, with the $P^{1/3}$ dependence persisting only at the lowest rigidities. The perpendicular MFPs at Earth remain well above the Palmer consensus values shown, again

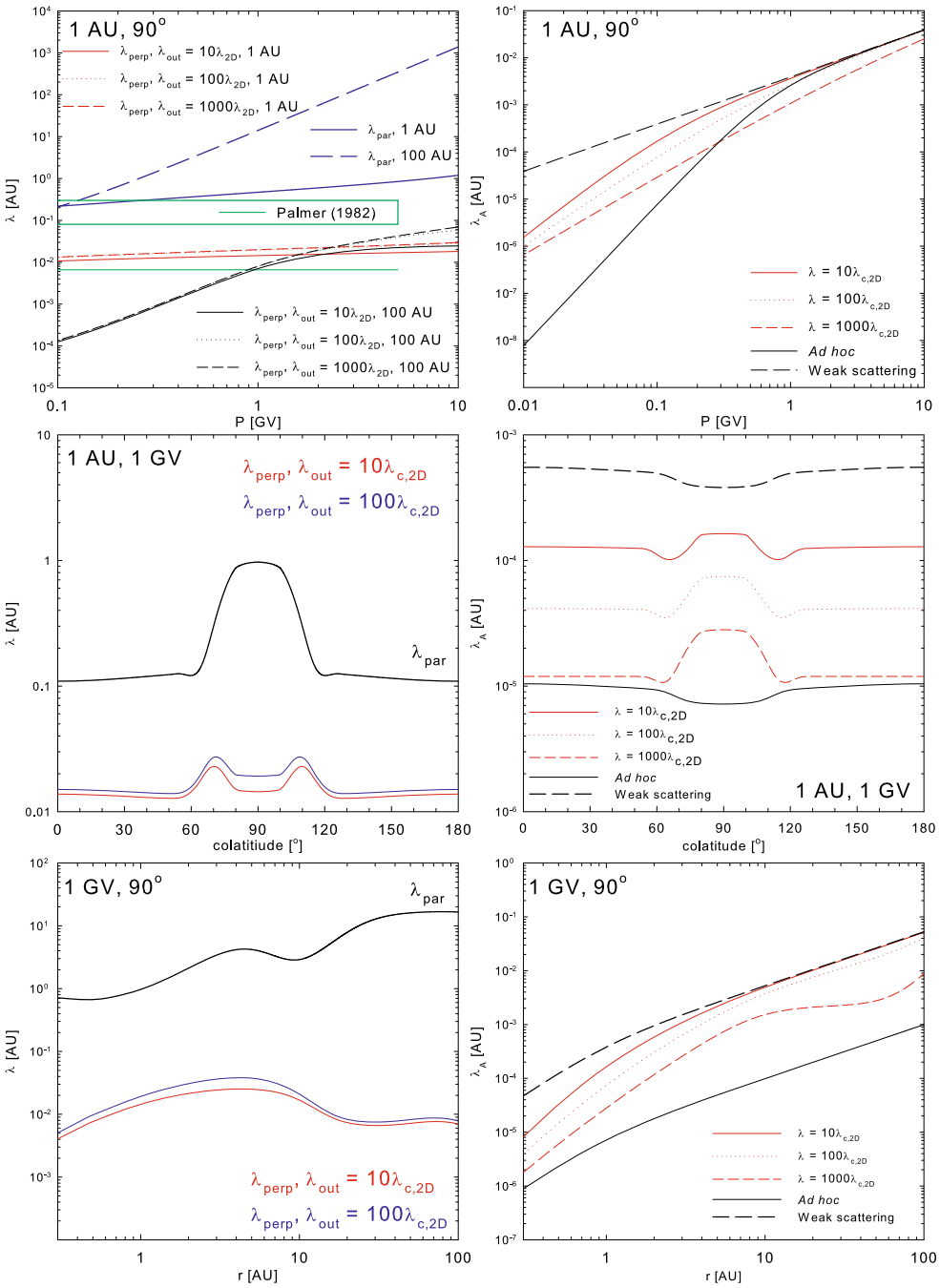

Fig. 3 MFPs and drift scales here considered, as functions of the 2D outerscale. *Top panels* show these quantities as functions of rigidity, *middle panels* as functions of colatitude and *bottom panels* as functions of heliocentric radial distance. The lengthscales in the bottom two panels are taken at 1 GV. Figure adapted from [12]

due to the solar minimum values yielded for the turbulence quantities used by the TTM, regardless of the value chosen for λ_{out}. These perpendicular mean free paths are somewhat similar to those presented by [31], with differences due to the single-component TTM employed in that study. All perpendicular MFPs at 1 AU display a relatively flat ($\sim P^{0.1}$) rigidity dependence, which is largely unaffected by the choice of outerscale. A larger value for λ_{out}, however, does lead to a larger value for $\lambda_{\perp}$, with values for the perpendicular mean free path approaching a limiting value as λ_{out} is increased. Due to this behaviour, only the cases where $\lambda_{out}=10\lambda_{c,2D}$ and $\lambda_{out}=100\lambda_{c,2D}$ will be shown when radial and colatitudinal dependences are discussed below. At 100 AU, the rigidity dependence of $\lambda_{\perp}$ changes. At the lowest rigidities, the perpendicular MFPs are very small, due to the very small 2D variances yielded by the [28] model at these large radial distances, and remain relatively unaffected by the choice of λ_{out}. The 100 AU perpendicular MFPs show an approximately P^2 rigidity dependence below ~1 GV, above which rigidity they either flatten out (for case where $\lambda_{out}=10\lambda_{c,2D}$) or display a $\sim P^{0.7}$ rigidity dependence (for the larger choices of 2D outerscale). This can be understood in terms of the analysis

[37] did of the NLGC perpendicular mean free paths they derived, showing that, when $\lambda_\perp\lambda_\parallel \ll 3\lambda_{2D}^2$, their perpendicular MFP would be proportional to the parallel MFP. When $\lambda_\perp\lambda_\parallel \gg 3\lambda_{2D}^2$, they showed that $\lambda_\perp \sim \lambda_\parallel^{1/3}$. The parallel MFP displays a P^2 dependence for most of the rigidities here considered at 100 AU, a rigidity dependence reflected in that of the ENLGC perpendicular MFPs below ~1 GV. The 1 AU perpendicular MFPs shown in the same figure scale as $\sim P^{0.1}$ due to the fact that, as modelled in this study, the quantity $3\lambda_{2D}^2$ is considerably smaller at 1 AU than it is at 100 AU, such that the condition $\lambda_\perp\lambda_\parallel \ll 3\lambda_{2D}^2$ is not satisfied at Earth. At 1 AU, however, and above ~1 GV at 100 AU, the condition $\lambda_\perp\lambda_\parallel \gg 3\lambda_{2D}^2$ is satisfied, leading to the rigidity dependences shown in Fig. 3, in line with a $\lambda_\perp \sim \lambda_\parallel^{1/3}$ dependency. The top right panel of Fig. 3 shows the drift scales as functions of rigidity, along with the weak scattering drift scale (equal to the Larmor radius), and an ad hoc drift scale used in previous studies (see, e.g. [9]). As larger values of λ_{out} are employed, the drift scales become smaller and remain below the weak scattering limit. For smaller values of the 2D outerscale, the drift scales approach the weak scattering values. The ad hoc drift scale agrees best with results for the smallest outerscale at high rigidity, but differs from it by an order of magnitude at the lowest rigidity shown.

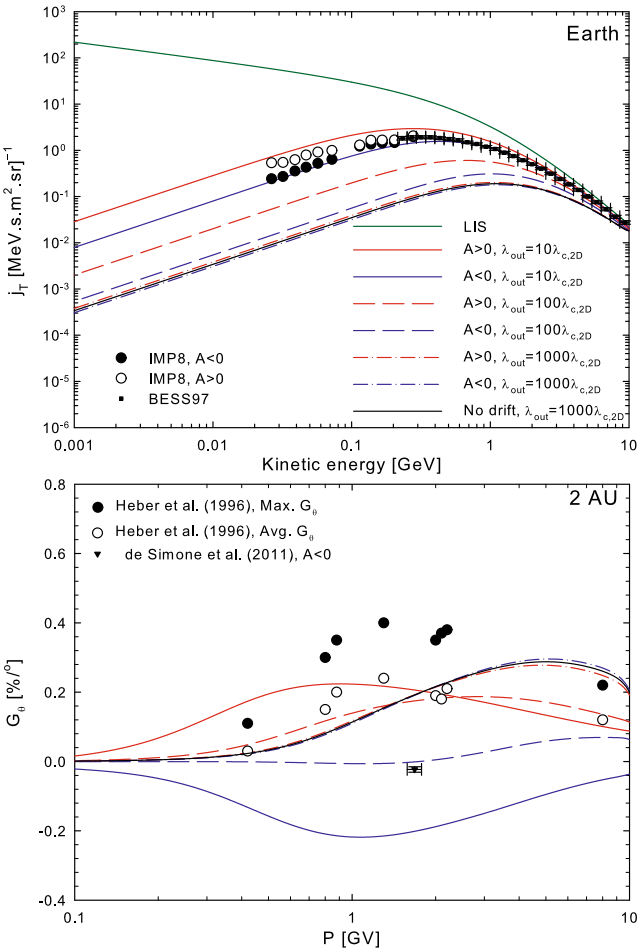

Fig. 4 Computed galactic proton intensities at Earth (*top panel*) and latitude gradients at 2 AU (*bottom panel*), as functions of the 2D outerscale. Figure adapted from [12]

Due to the use of the TTM, all lengthscales display spatial dependences more complicated than those considered in most previous studies. The parallel MFP, as function of colatitude, is very sensitive to the behaviour of the modelled slab variance, in that it assumes larger values in the ecliptic plane (with lower variances) than in the polar regions, in qualitative agreement with the observations of [14]. This is a consequence of the δB_{sl}^{-2} dependence of Eq. 9. The perpendicular MFP increases with increasing 2D variance and is hence also larger in the ecliptic than over the poles, with significant increases at colatitudes where stream-shear effects are modelled to be larger (see [6, 11] for more detail). A larger value for the 2D outerscale again leads to a larger value for $\lambda_\perp$. As functions of colatitude, the drift scales again follow the rule that the smallest drift scales correspond to the largest assumed values for the 2D outerscale. Drift scales are noticeably reduced at latitudes corresponding to regions of enhanced stream-shear effects where variances are greater, with drift scales corresponding to larger values of λ_{out} appearing to be more sensitive to these effects. The weak scattering and ad hoc drift scales tend to be smaller in the ecliptic than over the poles, following as they do the colatitudinal dependence of the Larmor radius, while for the [8] drift scales, the opposite is true, due to their dependence on the outputs of the TTM.

As function of radial distance, the parallel mean free path steadily increases until approx. 5 AU, beyond which a rapid decrease and flattening out is seen due to the changes in the slab variance and correlation scale caused by the ionization of interstellar neutral hydrogen, as modelled in the TTM. The perpendicular MFP also increases steadily with radial distance within 5 AU, following the behaviour of $\lambda_\parallel$. Beyond this distance, $\lambda_\perp$ remains relatively flat, in contrast to the steadily increasing perpendicular MFP presented by [31]. The differences between the radial dependence of the perpendicular MFP presented here and that of [31] are again due to the different TTMs employed. The choice of 2D outerscale appears to have a more significant effect for solutions in the inner heliosphere than at larger radial distances, with smaller values for λ_{out} leading to smaller $\lambda_\perp$. In the bottom right panel of Fig. 3, both the ad hoc and weak scattering drift scales follow the radial dependence of the proton gyroradius. The [8] drift scale for $\lambda_{out}=10\lambda_{c,2D}$ follows the weak scattering model most closely past ~10 AU, with larger values for the 2D outerscale yielding drift scales that no longer increase monotonically with increasing radial distance. Use of the largest outerscale leads to a drift scale with a radial dependence somewhat like that of the slab correlation scale, with smaller values of λ_{out} leading to drift scales more closely resembling the weak scattering limit.

4 Galactic Proton and Antiproton Modulation Results

Modulation results are acquired using a 3D, steady-state numerical modulation code [9, 11]. The proton local interstellar spectrum (LIS) here used is that of [9] while the antiproton LIS is that of [19], assuming a spherical heliosphere with a radius of 100 AU. The effects of a termination shock or heliosheath are not included. This is done because the [28] TTM was derived assuming an Alfvén speed considerably smaller than the solar wind speed, which is not the case in the heliosheath. Furthermore, a Parker HMF is assumed, using a latitude-dependent solar wind speed modelled with a hyperbolic tangent function that assumes a value of 400 km/s in the ecliptic and 800 km/s over the poles; the tilt angle of the heliospheric current sheet is taken to be 5° and the current sheet is treated following the approach of [7]. For more detail as to the choices here made for heliospheric parameters and their motivations, see [12, 11]. Figure 4 shows the computed galactic cosmicray proton intensities at Earth as functions of kinetic energy and their computed latitude gradients at 2 AU, for various choices of the 2D outerscale, as discussed in the previous section. The effects of the choice of 2D outerscale are very strong. This is because computed intensities depend quite strongly on the levels of drift reduction, which in turn depend quite strongly on the choice of λ_{out} employed. Larger intensities correspond to smaller choices for the 2D outerscale. This can be understood by considering the drift scales shown in Fig. 3, where choosing $\lambda_{out}=10\lambda_{c,2D}$ led to a drift scale closest to the weak scattering result. It is noteworthy that intensities computed assuming that $\lambda_{out}=10\lambda_{c,2D}$ almost fall on the IMP8 observations during $A>0$ and agree reasonably well with them during $A<0$. Intensities calculated under the assumption that $\lambda_{out}=1000\lambda_{c,2D}$ are very close to intensities calculated with the same choice for the 2D ultrascale, but with drifts turned off (solid black line in the top panel of Fig. 4). This is simply due to the small drift scales yielded by this choice of λ_{out}, as can be seen in Fig. 3. The choice of $\lambda_{out}=100\lambda_{c,2D}$ leads to intensities between those yielded by the $\lambda_{out}=10\lambda_{c,2D}$ and $\lambda_{out}=1000\lambda_{c,2D}$ scalings. From the bottom panel of Fig. 4, it can be seen that, regardless of the value assumed for the 2D outerscale in their calculation, the ab initio approach yields latitude gradients reasonably within the range of $A>0$ observations reported by [16], even though a Parker HMF model is used and perpendicular diffusion is assumed to be axisymmetric. During $A<0$, however, the latitude gradients computed assuming that $\lambda_{out}=10\lambda_{c,2D}$ and

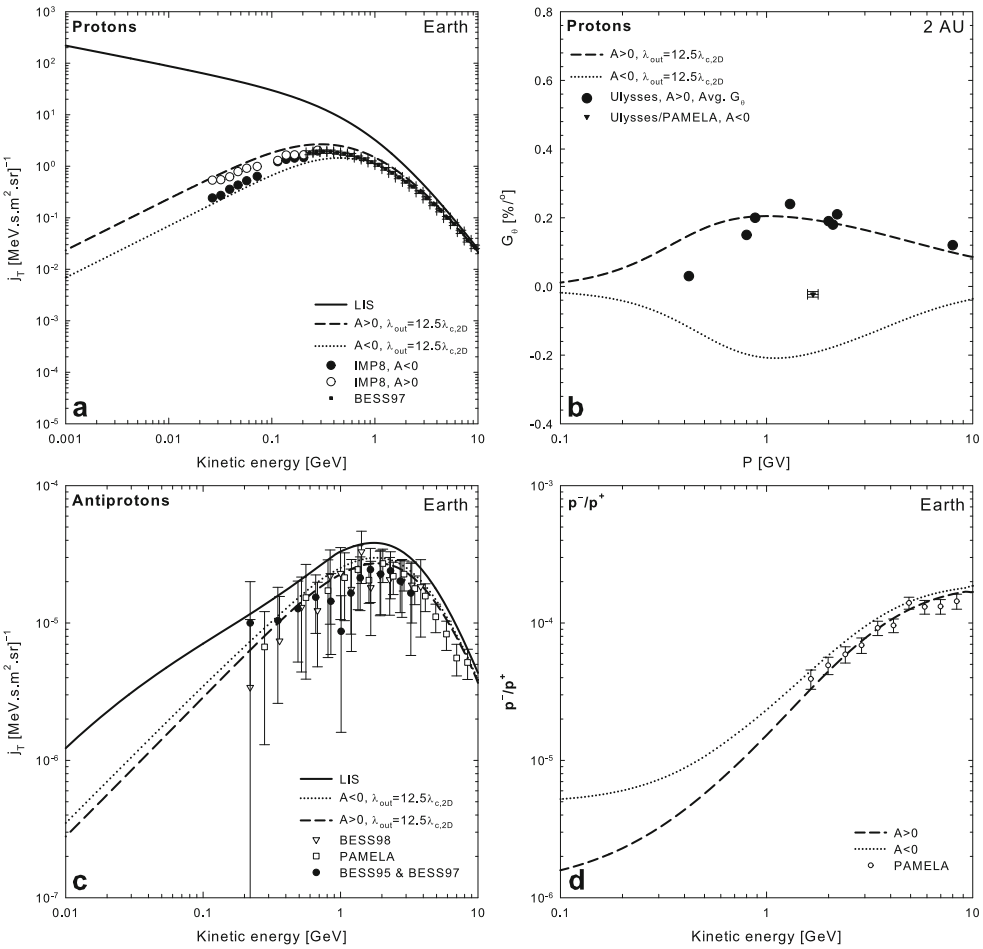

Fig. 5 Computed galactic proton intensities at Earth (*top left panel*) and latitude gradients at 2 AU (*top right panel*), along with computed antiproton intensities and the proton to antiproton fraction at Earth (*bottom left* and *right panels*, respectively). Figure taken from [11]

$\lambda_{out}=100\lambda_{c,2D}$ are negative, as expected [18], but tend to be too large when compared with the [10] observation. Assuming that $\lambda_{out}=1000\lambda_{c,2D}$ leads to positive latitude gradients for both magnetic polarity cycles, comparable to that calculated assuming no drift effects. This is again a consequence of the very small drift scales yielded by this choice of the 2D outerscale.

5 Conclusions

The [28] two-component turbulence transport model yields results in reasonable agreement with spacecraft observations at a variety of locations within the heliosphere. These results can be used as inputs for diffusion coefficients and drift reduction terms, which leads to complicated spatial dependences for these quantities. The perpendicular diffusion and drift coefficients, and by implication the computed cosmic ray intensities, are very sensitive to the choice made as to the 2D outerscale. Cosmic-ray intensities computed with this ab initio approach, using the same set of diffusion coefficients, are in reasonable agreement with multiple sets of spacecraft observations for protons and for antiprotons. This is illustrated in Fig. 5, which shows galactic proton and antiproton intensities computed by [11] using the same ab initio model, but assuming a 'best fit' scaling of $\lambda_{out}=12.5\lambda_{c,2D}$. Refinements to the model are, however, necessary and in the process of being made, but the fact that computed cosmic-ray intensities for galactic electrons and positrons are also in reasonable agreement with multiple sets of spacecraft observations (see, e.g. [13]) is very encouraging.

Acknowledgments The financial assistance of the National Research Foundation (NRF) towards this research is hereby acknowledged. Opinions expressed and conclusions arrived at, are those of the author and are not necessarily to be attributed to the NRF.

References

1. B. Bavassano et al., J. Geophys. Res. **105**, 15959–15964 (2000)
2. B. Bavassano et al., J. Geophys. Res. **105**, 12697–12704 (2000)
3. J.W. Bieber, W.H. Matthaeus, Astrophys. J. **485**, 655–659 (1997)
4. J.W. Bieber et al., Astrophys. J. **420**, 294–306 (1994)
5. B. Breech et al., Geophys. Res. Lett. **32**, 6103 (2005)
6. B. Breech et al., J. Geophys. Res. **113**, 8105 (2008)
7. R.A. Burger, Astrophys. J. **760**, 60 (2012)
8. R.A. Burger, D.J. Visser, Astrophys. J. **725**, 1366–1372 (2010)
9. R.A. Burger et al., Astrophys. J. **674**, 511–519 (2008)
10. N. de Simone et al., Astrophys. Space Sci. Trans. **7**, 425–434 (2011)
11. N.E. Engelbrecht, R.A. Burger, Astrophys. J. **772**, 46–57 (2013)
12. N.E. Engelbrecht, On the development and applications of a three-dimensional *ab initio* cosmicray modulation model, PhD Thesis, North-West University (2013)
13. N.E. Engelbrecht, R.A. Burger, An ab initio approach to the modulation of galactic electrons and positrons, Proceedings of the 33rd ICRC, Abstract 791 (2013b)
14. G. Erdös, A. Balogh, Adv. Space Res. **35**, 625–635 (2005)
15. L.J. Gleeson, W.I. Axford, Astrophys. J. **154**, 1011 (1968)
16. B. Heber et al., Astron. Astrophys. **316**, 538–546 (1996)
17. J.R. Jokipii, Astrophys. J. **146**, 480–487 (1966)
18. J.R. Jokipii, B. Thomas, Astrophys. J. **243**, 1115–1122 (1981)
19. U.W. Langner, M.S. Potgieter, J. Geophys. Res. **109**, 1103 (2004)
20. W.H. Matthaeus et al., Phys. Rev. Lett. **75**, 2136–2139 (1995)
21. W.H. Matthaeus et al., Phys. Rev. Lett. **82**, 3444–3447 (1999)
22. W.H. Matthaeus et al., Astrophys. J. Lett. **590**, L53–L56 (2003)
23. W.H. Matthaeus et al., Phys. Rev. Lett. **95**, 231101 (2005)
24. W.H. Matthaeus et al., Astrophys. J. **667**, 956–962 (2007)
25. J. Minnie et al., Astrophys. J. **663**, 1049–1054
26. J. Minnie et al., Astrophys. J. **670**, 1149–1158
27. H. Moraal, Space Sci. Rev. **176**, 299–319 (2013)
28. S. Oughton et al., J. Geophys. Res. **116**, 8105 (2011)
29. I.D. Palmer, Rev. Geophys. Space Phys. **20**, 335–351 (1982)
30. E.N. Parker, Planet Space Sci. **13**, 9–49 (1965)
31. C. Pei et al., J. Geophys. Res. **115**, 3103 (2010)
32. G. Qin et al., Geophys. Res. Lett. **29**, 1048-(2002)
33. D.A. Roberts et al., J. Geophys. Res. **92**, 12023–12035 (1987)
34. D.A. Roberts et al., J. Geophys. Res. **92**, 11021–11040 (1987)
35. A. Shalchi, Astron. Astrophys. **453**, L43–L46 (2006)
36. A. Shalchi, *Nonlinear cosmic ray diffusion theories* (Springer, Berlin, 2009)
37. A. Shalchi et al., Astrophys. J. **604**, 675–686 (2004)
38. W.S. Smith et al., J. Geophys. Res. **106**, 8253–8272 (2001)
39. C.W. Smith et al., Astrophys. J. Lett. **645**, L85–L88 (2006)
40. A. Teufel, R. Schlickeiser, Astron. Astrophys. **397**, 15–25 (2003)
41. J.M. Weygand et al., J. Geophys. Res. **114**, 7213 (2009)
42. J.M. Weygand et al., J. Geophys. Res. **116** (2011)
43. G.P. Zank et al., J. Geophys. Res. **101**, 17093–17107 (1996)